Available online at www.sciencedirect.com
ScienceDirect
Applied Catalysis A: General 323 (2007) 66–76
APPLIED CATALYSIS A: GENERAL
www.elsevier.com/locate/apcata

Mass and heat transfer effects on the oxidative dehydrogenation of propane (ODP) over a low loaded VO_x/Al_2O_3 catalyst

Benjamin Frank [a], Arne Dinse [a], Olga Ovsitser [b], Evgueni V. Kondratenko [b], Reinhard Schomäcker [a,*]

[a] *Department of Chemistry, Technical University of Berlin, Straße des 17. Juni 124, D-10623 Berlin, Germany*
[b] *Leibniz Institute of Catalysis at the University Rostock, Branch Berlin, Richard-Willstätter-Str. 12, D-12489 Berlin, Germany*

Received 2 November 2006; received in revised form 2 February 2007; accepted 2 February 2007
Available online 13 February 2007

Abstract

A low loaded VO_x/Al_2O_3 catalyst (1.4 wt.% V) was prepared by saturation-impregnation of a commercial γ-alumina support. The nature, distribution and redox properties of surface VO_x species were investigated by means of in situ UV–vis and TPR tests as well as by O_2 pulse experiments. Macroscopic structural properties of the catalyst were determined from XRD and BET (N_2 physisorption) analysis including pore size distribution. It was found that propene selectivity in the oxidative dehydrogenation of propane with oxygen in the temperature range of 673–773 K decreases with an increase in the size of the catalyst particles. Based on a simulation of intraparticle concentration and temperature profiles using developed intrinsic power-law kinetics, it was concluded that the dependence of propene selectivity on particle size is related to propene accumulation inside the particle pores and further oxidation. The kinetic evaluation indicated that total propene selectivity suffers exclusively from consecutive propene combustion to CO and CO_2, whereas the reaction of propane with lattice oxygen of VO_x species selectively yields propene. Moreover, the kinetic model in agreement with the experiment predicts an increase in propene selectivity with temperature. This is due to slightly higher activation energy of propene formation than its combustion. Since the measured effects were predicted quantitatively by the kinetic model, it, therefore, can be used for a precise design of extended microkinetic studies with this catalyst.

Keywords: Vanadia; VO_x/Al_2O_3; Oxidative dehydrogenation of propane; ODP; Kinetic model; Mass transport limitation; Particle modelling

1. Introduction

With increasing oil prices an alternative process for the production of lower alkenes is economically reasonable. An attractive reaction route instead of steam cracking of naphtha or catalytic cracking/dehydrogenation [1] is described by oxidative dehydrogenation, e.g. of propane (ODP). This alternative process is energetically favoured due to lower process temperatures and enhanced catalyst lifetime by the prevention of coke deposition. Furthermore, it is neither the equilibrium limited nor endothermic and therefore provides important advantages compared to established processes. Due to the increasing world demand for propene, the ODP reaction is a great challenge for catalysis research and development, and growing attention has been focused on this topic in the past decade. However, a low selectivity towards the desired product states the fundamental problem with respect to an industrial application up to now. The higher reactivity of propene in comparison to propane in oxidation reactions results in a fast consecutive propene combustion, which is the main limiting factor in the product yield.

A wide variety of catalysts and support materials have been investigated in the ODP reaction so far. Vanadia-based systems have been found to be the most active ones [2], due to their ability to change the oxidation state of vanadium between +III and +V quite easily. Unfortunately, there is a lack of comparable microkinetic data for a certain range of support materials and surface concentrations of vanadia in order to establish proper relationships between selectivity/activity and structural properties of catalysts. The impact of the support material and the vanadia concentration on the morphology of the vanadia species is remarkable [3,4] and so is its influence on

* Corresponding author. Fax: +49 30 31421595.
E-mail address: schomaecker@tu-berlin.de (R. Schomäcker).

0926-860X/$ – see front matter © 2007 Elsevier B.V. All rights reserved.
doi:10.1016/j.apcata.2007.02.006

the complex kinetics of the ODP reaction [5,6], which may thereby be used as a sensitive tool for the analysis of structure and chemical state of the catalytically active species. The investigation of this structure–activity relationship is one of the aims of the collaborative research center ''Structure, dynamics and reactivity of transition metal oxide aggregates'', funded by the German Research Foundation. The focus in our project is on the kinetic modelling and understanding of the reaction mechanism depending on the catalyst morphology with the future perspective to identify selective structures and develop improved catalysts. Vanadia deposited on γ-alumina was chosen as first candidate for an extensive microkinetic study. Common support materials as SiO_2, TiO_2 and ZrO_2 are planned for future investigations. In order to compare the kinetic data to quantum mechanical predictions, this data has to be gained from quasi-ideal model catalysts with a homogeneous structure. Deposited tetrahedral vanadia units tend to first oligomerize, polymerize and then form crystalline phases of V_2O_5 at higher surface concentrations [2,7]. Hence there exist three possible model systems of VO_x/Al_2O_3, which are relatively easy to prepare: (i) isolated monomeric species; (ii) a homogeneous monolayer; (iii) a bulk phase of VO_x. Since it is obvious that the impact of the support material is relatively weak in bulk species, the monomeric species were chosen due to their higher selectivity in the ODP reaction [8,9] and an easier preparation method. Moreover, a low vanadia surface concentration allows for less heat production per catalyst volume and therefore more isothermic reaction conditions, which are easier to investigate. One negative aspect of low loaded alumina-supported vanadia catalysts may be the reactivity of acidic alumina, which is, however, relatively low compared to VO_x species, and also much less selective [10,11].

The ODP reaction is a complex reaction network containing predominantly the following parallel and consecutive reactions [12,13]:

$$C_3H_{8(g)} + [\overset{+V}{V}O]_{(S)} \rightarrow C_3H_{6(g)} + H_2O_{(g)} + [\overset{+III}{V}]_{(S)} \quad (1)$$

$$C_3H_{8(g)} + (4+3x)[\overset{+V}{V}O]_{(S)} \rightarrow 3CO_{x(g)} + 4H_2O_{(g)} + (4+3x)[\overset{+III}{V}]_{(S)} \quad (2)$$

$$C_3H_{6(g)} + (3+3x)[\overset{+V}{V}O]_{(S)} \rightarrow 3CO_{x(g)} + 3H_2O_{(g)} + (3+3x)[\overset{+III}{V}]_{(S)} \quad (3)$$

$$CO_{(g)} + [\overset{+V}{V}O]_{(S)} \rightarrow CO_{2(g)} + [\overset{+III}{V}]_{(S)} \quad (4)$$

$$O_{2(g)} + 2[\overset{+III}{V}]_{(S)} \rightarrow 2[\overset{+V}{V}O]_{(S)} \quad (5)$$

Homogeneous contributions to this reaction scheme were observed only at temperatures above 773 K [14]. The reaction scheme depicted in Eqs. (1)–(5) represents a Mars–van Krevelen redox mechanism [15], which is generally accepted for oxidation reactions over vanadia catalysts [16]. The participation of lattice oxygen of VO_x species was proven in several studies [17–20]. Kinetic models were presented for several catalytic systems with more or less complexity up to now [12,13,21–23]. The precise determination of kinetic parameters suffers from the exothermicity, especially of reactions (2) and (3). The resulting axial temperature profile in case of usual fixed bed reactors can be reduced partly by catalyst or reactant dilution but isothermic conditions can only be approximated at propane conversions less than a few per cent of the feed. For experimental series with higher propane conversions the heat production has to be considered unavoidably for precise modelling. Produced reaction heat can also lead strong acceleration of the reaction and therefore to mass transfer limitations in the catalyst particle resulting in concentration and temperature profiles. These factors make a detailed integral kinetic evaluation impossible.

This paper states a basis for extensive microkinetic investigations with the low loaded VO_x/Al_2O_3 catalyst introduced in the present study. The limitations of microkinetic evaluable reaction conditions for the studied catalyst on the one hand and of usual tubular reactors on the other hand were determined. A simple formal kinetic model for the detailed design of further experiments in gradientless Berty-type reactor was established. The evaluation of the experiments contains the modelling of temperature and concentration profiles inside the catalyst particles as well as axial gradients over the reactor length.

2. Experimental

2.1. Catalyst preparation

The VO_x/Al_2O_3 catalyst was prepared by wet saturation-impregnation of a porous γ-alumina catalyst support (Alfa Aesar, item no. 43857) according to [9]. Prior to the impregnation, the alumina pellets were crushed and sieved to the following particle size fractions: 0.1–0.3, 0.3–0.6, 0.6–1.0, 1.0–1.5 and 1.5–2.5 mm, denoted in the following as VA-200, VA-450, VA-800, VA-1250 and VA-2000, respectively. A 0.1 mol l^{-1} solution of vanadyl acetylacetonate (Sigma–Aldrich, >97%) in toluene was heated under reflux until the boiling point was reached. For each catalyst sample, 2 g of the support was added slowly to 100 ml of the mixture and boiled under reflux for about 5 h. The impregnated particles were thoroughly washed with fresh toluene to remove unbound vanadyl species, then dried at 353 K for 12 h and finally, calcined in air at 773 K for 3 h. The calcined catalysts were sieved again to remove abrasion.

2.2. Catalyst characterization

When crushed and sieved to a particle diameter of 0.1–0.3 mm, all of the catalyst samples provided the same intrinsic activity and selectivity. The amount and the distribution of vanadia precipitated on the surface were thereby assumed to be

identical in all of the particle size fractions. Further detailed catalysts characterization was reduced to the sample VA-200.

The surface and pore size distribution of catalyst and support was determined via *nitrogen adsorption–desorption* at liquid nitrogen temperature (77 K), using a Micromeritics 2375 BET device equipped with a Vacprep 061 degasser. Before the measurement, the sample was degassed at 573 K for 1 h and 0.15 mbar in order to ensure a clean and dry surface. Surface area and pore diameters were calculated using the method of Brunauer, Emmett and Teller (BET).

Powder X-ray diffraction (XRD) measurements were conducted in order to get information about crystalline phases and crystallite size in the catalyst. The XRD patterns of catalyst samples and the support materials were obtained using a Siemens D500 instrument with monochromatic Cu Kα radiation, a scanning angle (2θ) range of 19–55°, a scanning speed of $8.3 \times 10^{-4\circ}\ s^{-1}$ and a voltage and current of 40 kV and 30 mA, respectively.

The total vanadium concentration (wt.%) of the catalyst was determined by *inductively coupled plasma spectroscopy* (ICP) using an ISA Jobin Yvon instrument. The sample was prepared for analysis by dissolving VO_x species from the freshly calcined catalyst with aqua regia.

Diffuse reflectance UV–vis spectroscopy (UV–vis DRS) was applied in order to investigate the nature of the vanadia species deposited on the alumina support. The in situ UV–vis analysis was performed using an AVASPEC fiber optical spectrometer (Avantes) equipped with a DH-2000 deuterium-halogen light source and a CCD array detector. A high-temperature reflection probe consisting of six radiating and one reading optical fibers was located inside the furnace perpendicular to the reactor. The sensor was connected to the spectrometer and the light source by fiber optical cables (length 2 m) consisting of a core of pure silica (diameter 0.4 mm) coated with polyimide.

Temperature-programmed reduction (TPR) measurements were performed by heating 200 mg of sample with 10 K min^{-1} up to 1073 K in a gas mixture of hydrogen (5 vol% in argon) with a total flow rate of 50 $ml_n\ min^{-1}$. Hydrogen consumption was monitored by mass spectrometry (Balzer Omnistar). Before TPR tests, the sample was heated (heating rate 20 K min^{-1}) in an oxygen flow (50 $ml_n\ min^{-1}$, 20 vol% in neon) up to 773 K for 0.5 h followed by cooling down to 323 K in the same flow. Hereafter, the O_2-treated sample was flushed with Ne for 0.25 h followed by feeding of hydrogen (beginning of TPR).

O_2-titration experiments were performed in the following way. After reaching 1073 K in TPR tests, the sample was cooled down to 773 K in the same reducing flow. O_2 pulse experiments were performed after flushing the reduced sample with Ne at 773 K for 0.2 h. O_2 pulse size was fixed to ca. 7 μmol.

2.3. Catalytic testing

The catalytic measurements were performed in a six-channel screening-apparatus at ambient pressure with U-shaped fixed bed quartz reactors (6 mm i.d.) connected in parallel. The catalyst particles were diluted with inert quartz sand in the mass ratio of 1:1. The feed consisted of synthetic air (20.5% O_2 in N_2) and propane, which were mixed in a composition to yield the stochiometric ratio of propane to oxygen of 2 for the ODP reaction (29.1% C_3H_8, 14.5% O_2, 56.4% N_2). Pure oxygen and nitrogen were used only in case of variation of the partial pressures of the reactants. The total gas flows were adjusted in the range of 30–240 $ml_n\ min^{-1}$ per channel. The reactant mixture passed a static mixer and was pre-heated up to 423 K prior to entering the reactor. The reactors, containing the diluted catalyst between two layers of quartz particles, were immersed into a fluidized bed of sand serving as a source of heat to provide near isothermal operating conditions. The reaction temperature was measured in a separate quartz tube placed in a position of the sand bed, which is comparable to that of the catalyst. For the measurement of the temperature profile inside the catalyst bed during the reaction, a special reactor was designed, containing an axially movable thermocouple located in a quartz capillary in the center. The feed and product components leaving the reactor were analyzed by an on-line gas chromatograph (GC, Satochrom 5873), equipped with Poraplot Q and Molsieve 5 columns. Light gases (O_2, N_2, CO, CH_4, CO_2) were detected with a thermal conductivity detector, C_2 and C_3 hydrocarbons and oxygenates were quantified using a flame ionization detector. The duration of one GC analysis was about 20 min, which is longer than the time to achieve steady state conditions, as confirmed by repeated measurements in one channel. Based on the inlet and outlet concentrations, the conversion of propane Eq. (6), and selectivity towards propene Eq. (7) were calculated. Using nitrogen as an internal standard, the reproducibility of conversion and selectivity measurement and calculation is sufficient (deviation <5% for the ODP reaction):

$$X = \frac{c_{C_3H_8,0} - c_{C_3H_8}}{c_{C_3H_8,0}} \tag{6}$$

$$S = \frac{c_{C_3H_6}}{c_{C_3H_8,0} - c_{C_3H_8}} \tag{7}$$

where $c_{i,0}$ and c_i are propane/propene concentrations at the reactor inlet and outlet, respectively.

Initial reaction rates of propane and propene conversion for the determination of activation energies and reaction orders were approximated by the concentration difference at low space-times t in kg s m^{-3}:

$$r_i = \frac{\Delta c_i}{t} \tag{8}$$

These space-times were adjusted for achieving propane conversions of less than 2%, which allowed the determination of the initial propene selectivity and the initial rates of product formation. Several experimental series were carried out in order to determine mass transport limitations, activation energies, reaction orders and rate constants of the main and consecutive reactions, respectively.

Numerical integration of reaction rates and heat production was conducted using a 4th order Runge–Kutta algorithm

included in the software package ''Berkeley Madonna 8.3.6''. Experimental data was fitted by the method of least square error (LSE).

3. Results and discussion

3.1. Catalyst characterization

The preparation method was designed for the deposition of well-dispersed VO_x monomeric species on the alumina surface, which is known to be appropriate to highly dispersed deposition [24]. The organic ligand acetylacetonate is relatively bulky and was chosen in order to prevent the adsorption of directly neighboured vanadium atoms. The presence of at least one of the ligands on the uncalcined catalyst is assumed from the dark colour of the precursor compared to support and calcined catalyst. Since following experiments showed that the duration of impregnation from 15 min up to 8 h has no effect on the catalytic activity, the surface may be regarded as homogeneously covered and ''saturated'' with vanadia species corresponding to this preparation method. This is advantageous to the highly reproducible preparation of adequate amounts of catalyst material for further studies.

The pale yellow catalyst grains had a BET surface of 106.6 $m^2\ g^{-1}$ and were found to be mesoporous with a medium pore diameter of 15.7 nm. These values are almost identical to that of the not impregnated catalyst support. The pore size distribution of both catalyst and support is given in Fig. 1(a). As can be seen from the similar shapes of the curves, there is a little clogging of micropores <5 nm observable but the support structure seems to be unaffected by the deposition of vanadia. Both catalyst and support material provided a high porosity of about 0.65 which was determined from the measured micropore volume.

The baseline-corrected XRD patterns of the powdered catalyst, the γ-Al_2O_3 support material, and crystalline V_2O_5 powder are presented in Fig. 1(b). One can see that there is no difference in the XRD patterns of the catalyst and the support. Moreover, any reflexes related to crystalline bulk vanadia phase are absent. This may be understood either as the presence of small crystalline V_2O_5 nanoparticles (<4 nm) or as surface VO_x species that cannot be detected by XRD due to the absence of long-range order. Based on the below UV–vis and H_2-TPR results, the presence of small crystalline V_2O_5 nanoparticles can be excluded. For deriving insights into the distribution of surface VO_x species, apparent density of vanadium (V nm^{-2}) was calculated from the BET value and vanadium loading. The total vanadia surface concentration was calculated from the results of the ICP experiments, which gave a content of 1.4 wt.% V in the catalyst. This leads to the apparent density of vanadium of 1.55 vanadium atoms nm^{-2} or 0.21 theoretical monolayers corresponding to the value of 7–8 VO_x nm^{-2} from Raman spectroscopy measurements [25,26]. This is in good agreement with the calculated value for a monolayer coverage with isolated monovanadates of 2.3 VO_x nm^{-2} [27]. Further insights into the degree of polymerization of surface VO_x species were derived from in situ UV–vis analysis. The results are described below.

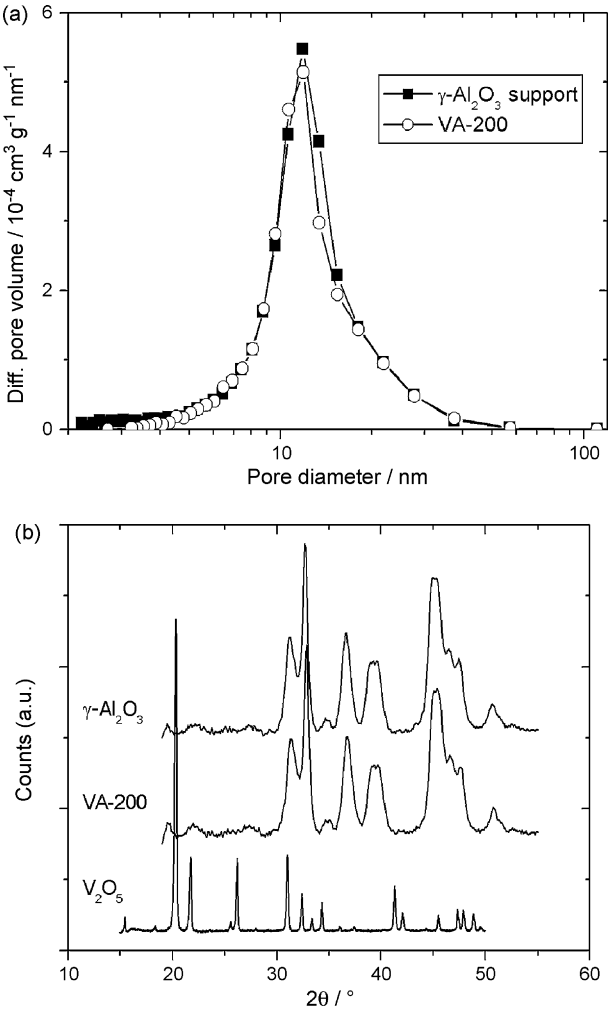

Fig. 1. (a) Pore size distributions of γ-Al_2O_3 support and catalyst VA-200; (b) powder XRD spectra of catalyst VA-200, γ-Al_2O_3 support and crystalline V_2O_5.

The UV–vis spectra of fresh and dehydrated (oxidized in an O_2 flow at 773 K) VA-200 catalyst are presented in Fig. 2(a). Both samples exhibit charge-transfer (CT) bands below 500 nm. However, the intensity of these bands is higher for the oxidized sample as compared to the fresh one. The difference is due to the fact that the fresh sample contained reduced VO_x species, which were oxidized to V^{5+} during the O_2 pretreatment at 773 K for 0.5 h. Small amounts of V^{4+} in the oxidized sample cannot be completely excluded. In order to derive insights into the structure/distribution of surface VO_x species in the oxidized VA-200 sample, its UV–vis spectrum was compared to that of VO_x (2.7 wt.%)/MCM-41, where isolated VO_4 units and small VO_x aggregates having V–O–V bonds are present on the surface [9]. The comparison is presented in Fig. 2(b). It can be seen that the height-normalized UV–vis spectrum of the oxidized VA-200 sample is slightly broader than that of the VO_x (2.7 wt.%)/MCM-41 sample. This broadening of the UV–vis spectra can be due to an increase in the domain size of VO_x species in the former sample as compared to the latter one. It appears that the VA-200 sample

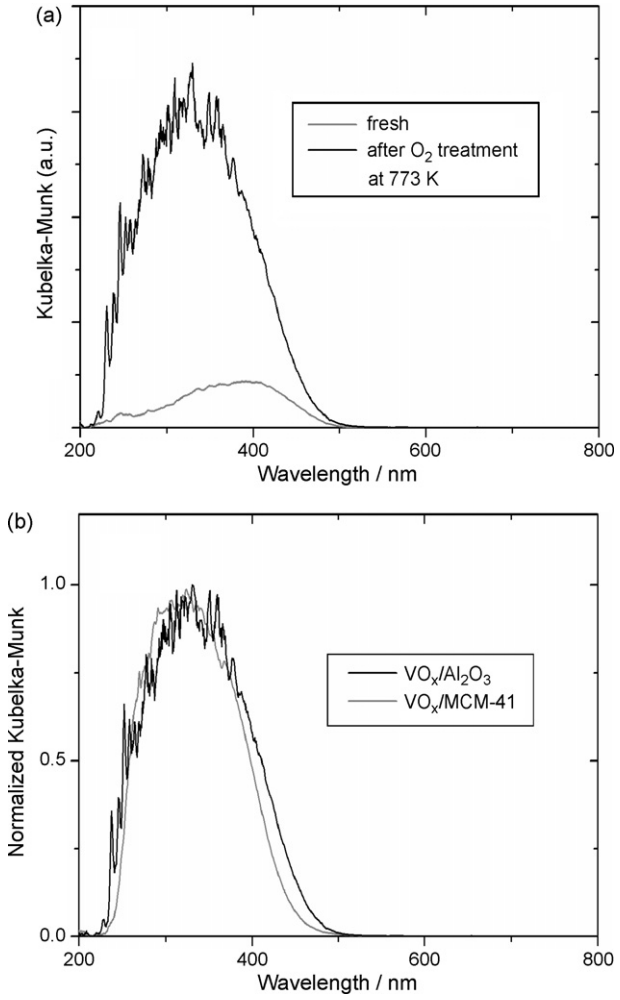

Fig. 2. (a) UV–vis DRS spectra of fresh and dehydrated VA-200 catalyst; (b) normalized UV–vis DRS spectra of dehydrated VO_x (2.7 wt.%)/MCM-41 and VA-200 catalysts.

possesses small amount of VO_x species with a higher degree of polymerization or domain size. However, the main VO_x species are highly dispersed.

To derive basic insights into the redox properties of surface VO_x species, the VA-200 material was tested by temperature-programmed reduction (TPR) in a hydrogen (5% H_2 in Ar) flow. The respective concentration profiles of H_2 and formed H_2O are presented in Fig. 3. At least two peaks of H_2 consumption were observed with maxima at ca. 560 and 800 K, respectively. Two distinct peaks of H_2O are also observed in similar temperature range. The presence of water indicates that H_2 is oxidized by lattice oxygen of VO_x species. In a previous study of some of the authors [11], only one maximum of H_2 consumption over VO_x (1 wt.%)/γ-Al_2O_3, which is similar to the VA-200 material, was detected at ca. 860 K. The discrepancy between these two studies can be related to the procedure of catalyst preparation; the VA-200 catalyst was prepared at 773 K, while the VO_x (1 wt.%)/γ-Al_2O_3 was calcined at 973 K. As shown by Steinfeldt et al. [7], the higher the calcination temperature, the higher the temperature of maximum of H_2 consumption. According to this previous work, it can be concluded that the

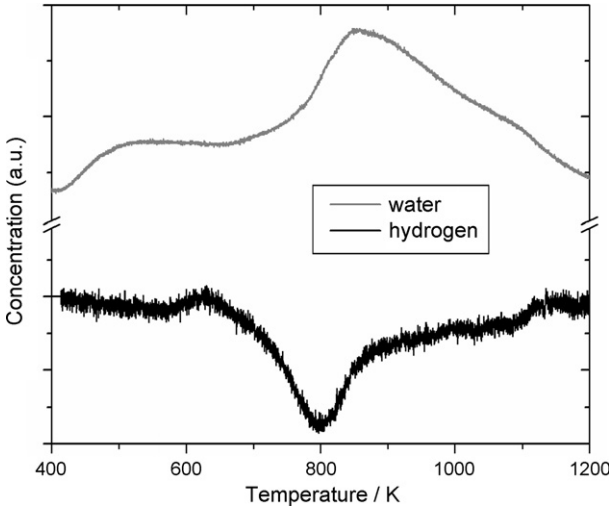

Fig. 3. H_2 and H_2O concentration profiles during temperature-programmed reduction of oxidizd VA-200 catalyst.

VA-200 catalyst does not contain microcrystalline V_2O_5, since no maxima of H_2 consumption were detected above 900 K.

The quantitative evaluation of the TPR profiles in Fig. 3 indicates that almost all V^{5+} species were reduced to V^{3+} assuming that the VA-200 catalyst possessed V^{5+} before the TPR test. The hydrogen amount consumed during TPR was 55 ± 5 μmol. This fits well with the amount of vanadium atoms, which was 55 μmol in this experimental series. In order to prove if the reduced VO_x species are reoxidized, O_2 pulse experiments were performed at 773 K after the TPR test (see Section 2). Only a part (ca. 40%) of reduced V^{3+} species was reoxidizd to V^{5+} or V^{4+}. The difference in the amount of lattice oxygen removed by H_2 in the temperature range of 423–1073 K and generated upon reoxidation of reduced VO_x species by O_2 at 773 K indicates that there are various VO_x species, which differ in their red–ox properties. However, structure of VO_x species and their red–ox properties can significantly change after TPR experiments at 1073 K. V^{3+} species generated by vanadia reduction may diffuse into the alumina lattice, and hence become non-available for the reoxidation step.

Summarizing the results of catalyst characterization, it can be concluded that the VA-200 catalyst possesses predominantly isolated VO_4 units, but the presence of minor amounts of VO_x aggregates having V–O–V bonds cannot be excluded. All these VO_x species are redox active.

3.2. Kinetic model and parameter estimation

Experiments for kinetic modelling were performed using the catalyst VA-200 with the smallest particle size fraction of 0.1–0.3 mm. As will be shown in Section 3.4, this is an essential requirement to avoid mass transport limitation of the reaction rate. Propane conversion and propene selectivity were measured at temperatures of 673, 723 and 773 K with a catalyst amount of 600, 110 and 50 mg, respectively. In order to achieve different degrees of propane conversion, the total gas

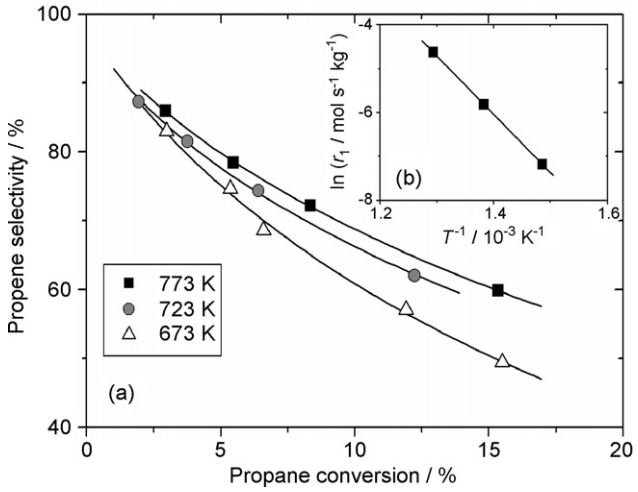

Fig. 4. (a) Propene selectivity as a function of propane conversion over catalyst VA-200; $C_3H_8/O_2/N_2 = 29.1/14.5/56.4$ and a total gas flow of 30–240 $ml_n\ min^{-1}$; (b) Arrhenius plot from initial rates of the ODP reaction, i.e. lowest conversion data from (a).

flow was varied between 30 and 240 $ml_n\ min^{-1}$. The resulting selectivity–conversion relationships are shown in Fig. 4 together with the Arrhenius plot from initial conversions measured with the highest flow rate of 240 $ml_n\ min^{-1}$. For all temperatures, propene selectivity decreases with an increase in propane conversion. This is due to a consecutive C_3H_6 oxidation to CO and CO_2. The ratio of CO/CO_2 was found to be 1.8–2 and independent on temperature and degree of propane conversion. Increasing temperature results in increased propene selectivity at similar degrees of propane conversion. This positive influence of temperature on propene selectivity is in agreement with previously reported results of the oxidative dehydrogenation of propane (ODP) over alumina-supported vanadia catalysts [3] and over a mixed vanadium-containing alumina-supported catalyst [19].

The catalyst VA-200 shows a high selectivity towards propene compared to samples prepared by a conventional incipient wetness impregnation method [8] in the same vanadia concentration range. This may indicate a difference in the vanadia distribution on the support due to the preparation method on the one hand or be related to the high porosity of the catalyst support of about 0.7 on the other hand, which allows efficient mass transport by diffusion.

Since the kinetic modelling presented here is required only to estimate the influence of mass and heat transport on the ODP reaction, a simplified power-law type kinetic model is applied, which contains no mechanistic information. The following simplifications concerning the reaction network in Eqs. (1)–(5) were made: (i) direct (not via consecutive propene oxidation) propane conversion to CO_x can be neglected, since near 100% propene selectivity at near zero propane conversion is expected from the selectivity–conversion relationships in Fig. 4; (ii) secondary oxidation of CO to CO_2 does not play any significant role, because the ratio of CO and CO_2 does not depend on the propane conversion. Taking the above simplifications into account the reaction network required for a sufficient fit simplifies to

$$C_3H_{8(g)} + [\overset{+V}{V}O]_{(S)} \rightarrow C_3H_{6(g)} + H_2O_{(g)} + [\overset{+III}{V}]_{(S)}$$

$$C_3H_{6(g)} + 7[\overset{+V}{V}O]_{(S)} \rightarrow 2CO_{(g)} + CO_{2(g)} + 3H_2O_g + 7[\overset{+III}{V}]_{(S)} \quad (3a)$$

$$O_{2(g)} + 2[\overset{+III}{V}]_{(S)} \rightarrow 2[\overset{+V}{V}O]_{(S)}$$

with the following rate laws for the oxidative dehydrogenation of propane (r_1) and consecutive propene combustion (r_3):

$$r_1 = k_{\infty,1} \exp\left(-\frac{E_{A,1}}{RT}\right) c_{C_3H_8}^{m_1} c_{O_2}^{m_2} \quad (9)$$

$$r_3 = k_{\infty,3} \exp\left(-\frac{E_{A,3}}{RT}\right) c_{C_3H_6}^{m_3} c_{O_2}^{m_4} \quad (10)$$

The parameters to be determined reduce to two preexponential factors k_∞, two apparent activation energies E_A and four reaction orders m_i. The apparent activation energy of the ODP reaction can be calculated from the lowest conversions given in Fig. 4, the value for propene combustion was measured in a somewhat lower temperature range of 633–678 K due to higher reaction rates. In case of gradientless reaction conditions for VA-200 up to 773 K (as will be shown in Section 3.4), this value can be adopted to the higher temperature range. Due to the enormous exothermicity of propene deep oxidation, the conversion of this reaction has to be adjusted at very low values (<3%) in order to exclude falsification of the initial rate data by temperature arise along the catalyst bed. The Arrhenius plot then shows linear correlations of $\ln(r_i)$ versus T^{-1} with excellent accuracy. The preexponential factors were not taken from this plot because the intercept contains also the concentration terms of the rate equations (9) and (10). The reaction orders were determined by varying the concentration of one reactant while keeping the other one constant at a temperature of 673 K. The composition ranges of $C_3H_8/O_2/N_2$ in vol% for the ODP reaction were varied between 40/2–40/balance and 20–60/20/balance, respectively. For propene combustion the following compositions of $C_3H_6/O_2/N_2$ in vol% were applied: 20–50/20/balance and 40/2–20/balance with a total gas flow of 100 $ml_n\ min^{-1}$ in each of the four experimental series. The reaction order of component j in reaction i is then given by the slope of $\ln(r_i)$ versus $\ln(c_j)$ where j is the component which was varied in its concentration. However, although the results of the ODP reaction could be linearized in a sufficient manner, the accuracy of the propene combustion reaction orders suffered probably from the high reaction exothermicity, which caused relatively high error bars on the measured conversions and thereby on m_3 and m_4. The resulting apparent activation energies and reaction orders are listed in Table 1. It can be seen that the apparent activation energy of the ODP reaction is slightly higher than that of propene combustion. This may be related to the stronger C–H bond in the propane molecule than in the propene molecule. The absolute values of $E_{A,i}$ as well as their difference $E_{A,1}$–$E_{A,3}$

Table 1
Kinetic parameters determined for the ODP reaction and propene combustion

Propene formation	
$k_{\infty,1}$	1.97×10^5 mol$^{0.25}$/m$^{-2.25}$ s kg
$E_{A,1}$	111 kJ mol^{-1}
m_1	0.65 ± 0.01
m_2	0.1 ± 0.002
Propene combustion	
$k_{\infty,3}$	9.43×10^4 mol$^{-0.70}$/m$^{-5.10}$ s kg
$E_{A,3}$	102 kJ mol^{-1}
m_3	0.7 ± 0.2
m_4	1.0 ± 0.2

are dependent on the vanadia content and are in moderate agreement with comparable literature data [3]. Based on the positive difference of $E_{A,1}$–$E_{A,3}$, an increase of propene selectivity with temperature can be expected and was experimentally observed (Fig. 4).

Both, for the ODP reaction and propene combustion, the reaction order with respect to propane and propene partial pressures is close to one. However, the reaction orders with respect to oxygen partial pressure are close to zero and to one for propane and propene oxidation, respectively. The reaction orders are in general comparable to another study [13], although this presented kinetic model could not reflect our measurements. A reason for the higher reaction order of oxygen in the propene combustion relative to the ODP reaction may be the higher overall reaction rate of propene combustion. This enhances the impact of catalyst reoxidation, based on the assumption that the rate of this elementary reaction step is independent from the reducing agent. Against that, the ODP reaction is relatively slow and the reoxidation rate seems to be nearly negligible in the overall reaction rate, expressed in a reaction order of nearly zero. The last missing parameters, the preexponential factors, were not calculated from the Arrhenius plot, due to the relatively high inaccuracy of the reaction orders especially of the propene combustion. The resulting error in k_∞ would be enhanced due to the exponential character of the Arrhenius plot, so these values were determined by the integral fit described in Section 3.3.

3.3. Modelling of the reaction on a tubular reactor

The U-shaped quartz reactor used in this study was modelled as ideal plug-flow tubular reactor (PFTR), which means that axial dispersion as well as radial temperature and concentration gradients were not taken into account. However, the calculated Bodenstein numbers in the range of 20–50 and Reynolds numbers in the range of 1–3 for this experimental study indicate the presence of residual backmixing effects and parabolic velocity profiles. Their influence on the measured reaction rate was estimated to be low and thereby was neglected in order to greatly simplify the kinetic evaluation. A narrow residence time distribution of the applied reactor set-up was tested and confirmed by independent tracer step marking before catalytic experiments.

Furthermore, the reaction mixture was set constant in volume, although the mole number of the reaction increases slightly with the conversion and so does the gas volume. This simplification is of no consequence because of the dilution of the reaction mixture with inert nitrogen, which weakens this effect. The following balances were used for the one-dimensional modelling of the experimental data presented in Fig. 4:

$$\frac{\mathrm{d}}{\mathrm{d}t} c_{C_3H_8} = -r_1 \tag{11}$$

$$\frac{\mathrm{d}}{\mathrm{d}t} c_{C_3H_6} = r_1 - r_3 \tag{12}$$

$$\frac{\mathrm{d}}{\mathrm{d}t} c_{O_2} = -0.5 r_1 - 3.5 r_3 \tag{13}$$

$$\frac{\mathrm{d}}{\mathrm{d}t} T = \frac{r_1 \Delta_R H_1 + r_3 \Delta_R H_3}{c_0 \bar{c}_p} - (T - T_W) \frac{k_W A_W}{V_R c_0 \bar{c}_p} \tag{14}$$

where $\Delta_R H_1 = 120$ kJ mol^{-1} and $\Delta_R H_3 = 1360$ kJ mol^{-1} are the enthalpies of reactions (1) and (3), respectively, c_0 the total gas concentration with the medium heat capacity $\bar{c}_p$, estimated from literature data [28], and T_W is the temperature of the fluidized sand bed. The ratio of the heat transfer area A_W and the reactor volume V_R is given by the reactors dimensions and equal to $2/r$ for cylindrical geometry. k_W is the overall heat transfer coefficient of the quartz wall of the reactor. The estimated value of $k_W = 3.4$ W m^{-2} K^{-1}, given by the experimental set-up and mainly limited by the inner convection heat transfer coefficient h of the reactor wall due to laminar flow conditions [28], allows a fit of concentration and temperature profiles in an excellent quality. Using these equations, the preexponential factors of rate Eqs. (9) and (10) were determined as given in Table 1. The axial temperature and concentration profiles of the reactor are illustrated in Fig. 5 exemplarily for $T = 773$ K.

As can be seen from the fit there are no remarkable hotspots in the reactor during this experiment. The absence of relevant

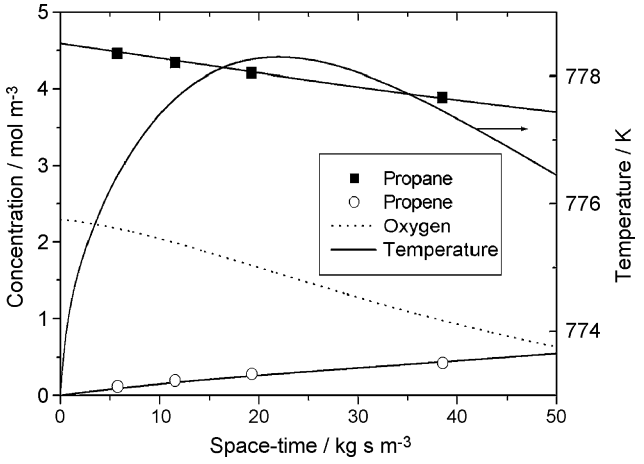

Fig. 5. Temperature and concentration profiles of propane, propene and oxygen during the ODP reaction over VA-200 using conventional quartz reactors; $C_3H_8/O_2/N_2 = 29.1/14.5/56.4$, $T_{in} = 773$ K and a total gas flow of 30–200 ml$_n$ min^{-1}.

temperature gradients may be referred to the low activity of the catalyst VA-200 and the dilution of the catalyst particles with inert quartz particles. The temperature maxima increase to values of 0.4, 1.1 and 5.3 K above the temperature of the fluidized sand bed in the experimental series conducted at 673, 723 and 773 K, which indicates an efficient heat transfer. The more pronounced maxima at higher temperatures are the result of the local heat production due to higher catalyst activity. Measurements with the reactor equipped with a centred thermocouple resulted in temperature peaks of 3 K in a diluted 50 mg catalyst bed at 773 K. At both of the lower reaction temperatures no temperature increase was detectable. This is in good agreement with the model, confirming the assumption of a moderate and controllable heat production in this system.

3.4. Investigation of mass transport effects

Mass transport effects are one of the most important error sources in a kinetic analysis of fast reactions and therefore have to be excluded before beginning a detailed investigation of reaction networks and microkinetics. Our further microkinetic investigations of the ODP reaction are planned to be performed in a Berty-type reactor. Since its gas-phase mixing quality is amongst others strongly dependent on the catalyst particle size, it is very essential to prove whether the ODP reaction is influenced by the size of catalyst particles. To this end, we studied the ODP reaction over differently sized $VO_x/\gamma\text{-}Al_2O_3$ samples (VA-200, VA-450, VA-800, VA-1250, and VA-2000) in the temperature range of 673–773 K. Fig. 6 illustrates the selectivity–conversion relationships obtained at 673, 723, and 773 K over these samples. Not depending on the size of catalyst particles propene selectivity decreases with an increase in the degree of propane conversion. However, the size of catalyst particles influences strongly the propene selectivity. The larger the particle size, the lower the propene selectivity. Moreover, the difference between differently sized catalyst particles in propene selectivity at a certain contact time depends on reaction temperature and increases with an increase in temperature. The observed effects of the particle size on the propene selectivity are explained by mass transport limitations inside of larger particles, i.e. reaction product is accumulated inside of larger particles due to a longer path for pore diffusion, which causes an acceleration of consecutive reactions [29]. Since propene combustion is faster than the ODP reaction, this effect occurs at noticeably smaller particle sizes than the observation of mass transport effects on the ODP reaction. The influence of mass transport limitations on propene selectivity decreases with decreasing temperature, because the rate of chemical reaction decreases stronger than diffusion inside catalyst particles. Thus in opposition to the tendency for nearly intrinsic kinetics as shown in Fig. 4, the selectivity then decreases with increasing temperature in case of mass transfer resistances.

Beside the effect on the overall propene selectivity, the initial (at near zero propane conversion) propene selectivity is also strongly influenced in the presence of diffusion limitations. It decreases significantly upon increasing size of catalyst particles. Compared to VA-200, where the intercept is near

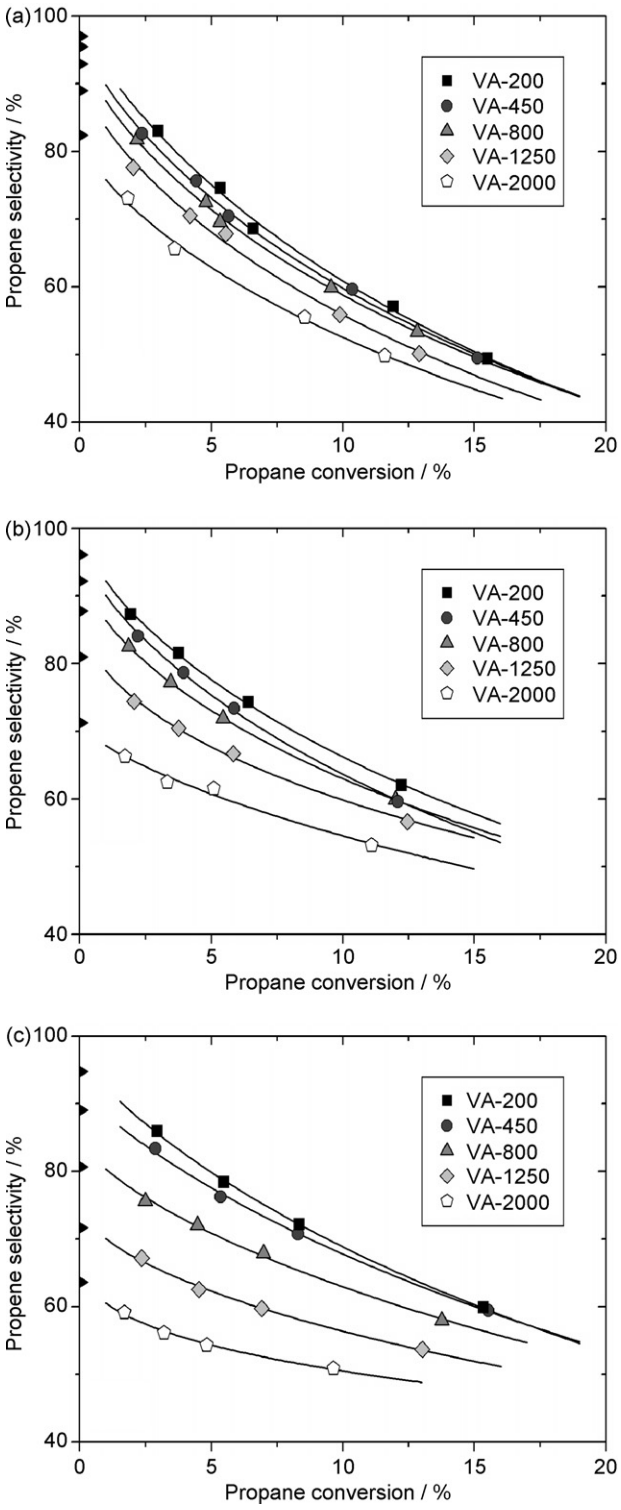

Fig. 6. *X*/*S*-trajectories of the ODP reaction over VA catalyst samples with different medium particle diameter; $C_3H_8/O_2/N_2 = 29.1/14.5/56.4$ and a total gas flow of 30–240 $ml_n\ min^{-1}$: (a) 673 K and 600 mg catalyst; (b) 723 K and 110 mg catalyst; (c) 773 K and 50 mg catalyst including simulated values (black triangles at the *S*-axis).

100% propene selectivity, this pretends a change in the reaction network and a parallel combustion pathway of propane. This effect may be explained by the accumulation of propene inside the catalyst pores and thereby an enhanced consecutive propene

combustion. The material balance at the particle surface then also contains a particle flux of CO_x leaving the particle even at differential propane conversion, which macroscopically may be misinterpretated as direct propane combustion. It should be also mentioned that the degree of propane conversion decreases with increasing particle diameter for a constant residence time. Reduced ODP reaction rates are the common effect of mass transport limitation.

In order to further analyze the effect of mass transport limitations on the ODP reaction, the interior balances for the catalyst particles were solved. The following conditions were assumed: (i) spherical geometry; (ii) gradients in the center of the particles are zero (symmetry criterion); (iii) reactant concentrations and temperature at the surface are equal to gas-phase concentrations and temperature, respectively. The latter means no outer mass transport limitation, which is provided by high gas flow rates at differential conversion (Maers criterion). Balances (15)–(18) were used for the intraparticle gradient simulation:

$$\frac{d^2}{dR^2}c_{C_3H_8} + \frac{2}{R}\frac{d}{dR}c_{C_3H_8} = \frac{\rho_{cat}}{D_{K,C_3H_8}}r_1 \quad (15)$$

$$\frac{d^2}{dR^2}c_{C_3H_6} + \frac{2}{R}\frac{d}{dR}c_{C_3H_6} = \frac{\rho_{cat}}{D_{K,C_3H_6}}(-r_1 + r_3) \quad (16)$$

$$\frac{d^2}{dR^2}c_{O_2} + \frac{2}{R}\frac{d}{dR}c_{O_2} = \frac{\rho_{cat}}{D_{K,O_2}}(0.5r_1 + 3.5r_3) \quad (17)$$

$$\frac{d^2}{dR^2}T + \frac{2}{R}\frac{d}{dR}T = \frac{\rho_{cat}}{\lambda^e}(r_1\Delta_R H_1 + r_3\Delta_R H_3) \quad (18)$$

where R is the particle radius, ρ_{cat} the catalyst density, $D_{K,i}$ the Knudsen diffusivity Eq. (19) and λ^e the effective heat conductivity of porous γ-alumina, estimated with 0.2 W m^{-1} K^{-1}:

$$D_{K,i} = \frac{\varepsilon}{\tau}\frac{d_p}{3}\sqrt{\frac{8RT}{\pi M_i}} \quad (19)$$

where ε and τ are the catalysts porosity and tortuosity, d_p the pore diameter and M_i the molar mass of component i. A typical value of 3.5 was taken for the tortuosity, whereas porosity and pore diameter were determined by BET experiments. The resulting gradients for VA-2000 at 773 K are exemplarily shown in Fig. 7. This figure nicely illustrates that the lowest concentration of propane and oxygen is expected in the middle of the particle. It increases with a decrease in the distance to the outer surface of the catalyst particle. The profile of propene concentration shows an inversed trend as compared to propane and oxygen; i.e. the lowest propene concentration is expected at the outer surface of the catalyst particle. The concentration gradients become smaller when the size of catalyst particles decreases as exemplified in Fig. 8(a) for O_2 concentration. This observation is due to an enhanced diffusion through the particle upon decreasing particle size. The smallest gradient were calculated for particles of 0.1–0.3 and 0.3–0.6 mm. This is in good correspondence to our experimental observations in Fig. 6. The measured propene selectivities over these two

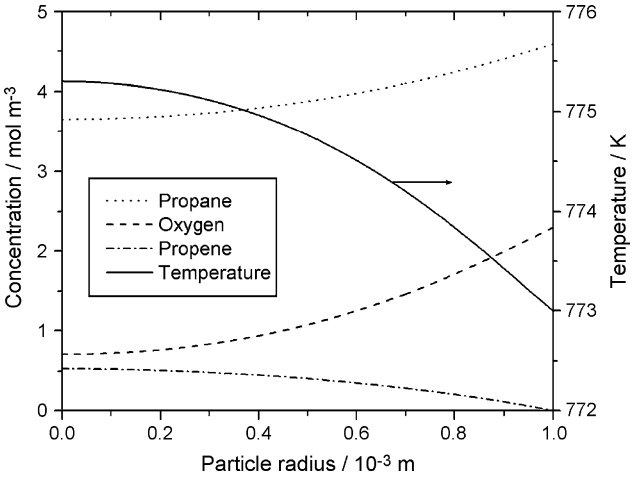

Fig. 7. Intraparticle concentration and temperature profiles simulated for a VA-2000 catalyst particle: initial reaction conditions: $C_3H_8/O_2/N_2$ = 29.1/14.5/56.4, T = 773 K.

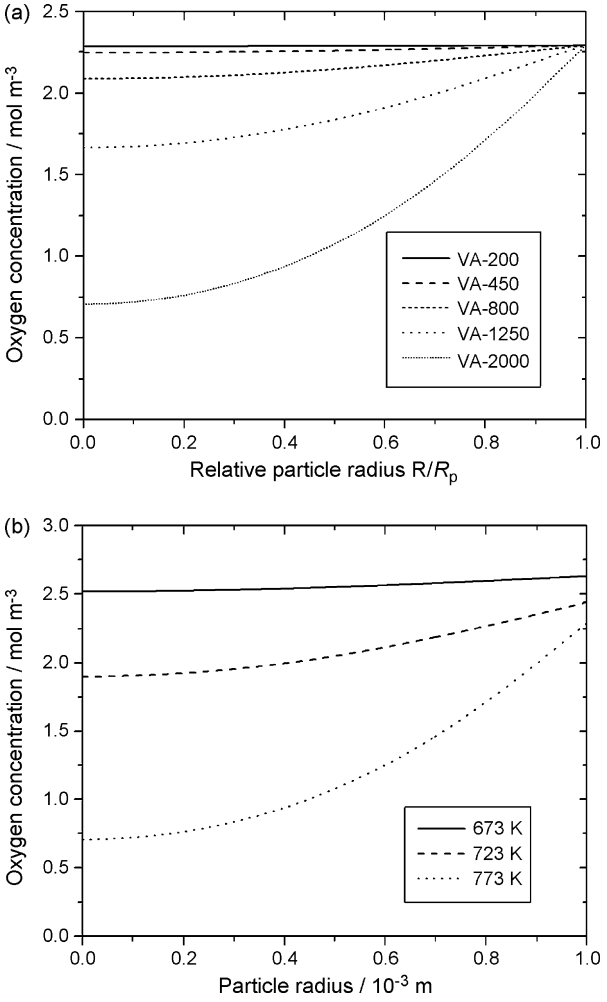

Fig. 8. Simulated intraparticle gradients of the oxygen concentration: (a) for different particle diameters at 773 K; (b) for different temperatures using VA-2000; $C_3H_8/O_2/N_2$ = 29.1/14.5/56.4, initial reaction conditions.

Table 2
Initial selectivities of the ODP reaction over the VO_x/Al_2O_3 catalyst, simulated (S_{sim}) with the spherical particle model and estimated (S_{est}) from extrapolation of experimental data given in Fig. 6 to zero propane conversion

Sample	VA-2000	VA-2000	VA-2000	VA-1250	VA-800	VA-450	VA-200
T (K)	673	723	773	773	773	773	773
S_{sim} (%)	82.4	71.3	63.6	71.7	80.7	89.1	94.7
S_{est} (%)	80	70	63	73	82	92	96

catalyst fractions were very similar in a broad range of propane conversions. Upon further increase in the size of catalyst particles, propene selectivity decreases (Fig. 6) and concentration gradient inside the catalyst particles significantly increases (Fig. 8(a)).

The effects of temperature on intraparticle gradients of reaction components were also calculated for the largest catalyst particles (1.5–2.5 mm). Fig. 8(b) exemplifies O_2 concentration profiles. It can be seen that the highest gradients were calculated at 773 K. They decrease upon decreasing reaction temperature. The difference between large and small catalyst particles in propene selectivity decreases in a similar manner. This is due to the fact the reaction rate decreases stronger with temperature than the diffusion. Therefore, the influence of mass transport on the ODP reaction decreases and the kinetic regime is reached at gradientless conditions.

Besides the visualization of intraparticle gradients, more information can be extracted from the modelling. The initial propene selectivity S is given by the ratio of the propene and propane concentration gradients at the catalyst particle surface:

$$S = -\frac{(\mathrm{d}/\mathrm{d}R)c_{C_3H_6}\Big|_{R=R_p}}{(\mathrm{d}/\mathrm{d}R)c_{C_3H_8}\Big|_{R=R_p}} \quad (20)$$

where R_p is the radius of the catalyst particles. The selectivities determined for VA-2000 at 673 and 723 K as well as for the whole VA-series at 773 K are assembled in Table 2. The predicted selectivities are in excellent agreement with the extrapolated values from Fig. 6(a–c), which are in the range of about 60–100%.

Summarizing, a manifold impact of mass transport limitation on activity, selectivity and the apparent reaction network could be identified in the present study. This conclusion is of high importance for deriving intrinsic kinetics of the ODP reaction and generally indicates the tremendous impact of this falsifying factor in kinetic studies.

4. Summary and conclusions

Macro-kinetic aspects of the oxidative dehydrogenation of propane (ODP) have been studied over a low loaded VO_x/Al_2O_3 in the temperature range of 673–773 K using catalyst particles of different size (0.1–2.5 mm). In the studied range of catalyst particles, it was found that the higher the particle size, the lower the propene selectivity at similar degrees of propane conversion. This is due to the appearance of mass transport limitations, which lead to product accumulation in the catalyst pores resulting in consecutive propene oxidation to CO_x. These limitations do not play significant role for catalyst particles up to 0.3 mm and temperatures up to 773 K. Since the ODP selectivity and the mass transport limitations increase with reaction temperature, it appears desirable to perform the reaction at highest possible reaction temperature using smallest possible catalyst particles. Taking this into account, microstructured reactors are suggested to be suitable candidates for such studies, because mass transport in these reactors has lower influence on the intrinsic kinetic as compared to conventional fixed bed reactor.

The kinetic parameters of the ODP reaction were determined under thorough exclusion of mass transport and heat effects, using a PFTR model and a power-law kinetic approach. The simplified model included propene formation from propane and a consecutive combustion of propene with a resulting ratio of CO to CO_2 of 2. This ratio was found to be nearly constant under the chosen reaction conditions. The model predicts the axial temperature profile of the reactor by inclusion of the heat transfer over the reactor wall. Moreover, the negative effects of particle size on the propene selectivity could be predicted nearly quantitatively with the kinetic model if applied in the material balance of a single catalyst particle with spherical geometry. These excellent agreements make this model a powerful tool to design further microkinetic investigations in a gradient less Berty-type reactor.

Although the applied catalyst was of relatively low activity as compared to most of the catalytic systems discussed in literature, it could not be completely excluded that the propene selectivity at 773 K was not affected by the mass transport limitations even at the smallest particle diameter (0.1 mm) investigated in this study. This knowledge may serve as a guideline for performing further ODP tests over more active catalysts. Moreover, by comparing literature data on various catalytic materials, it is of highly importance to critically analyze, whether the results reported in literature may be influenced by the mass transport limitations, if these aspects have not be explicitly discussed.

Acknowledgements

This work was supported by the German Research Foundation (Deutsche Forschungs-gemeinschaft, DFG) in the frame of the collaborative research center ‘‘Structure, dynamics and reactivity of transition metal oxide aggregates’’ (Sonderforschungsbereich 546, http://www.chemie.hu-berlin.de/sfb546). The authors

are furthermore grateful to Anja Ruch, Oliver Schwarz and Harald Link for experimental assistance.

References

[1] P. Eisele, R. Killpack, Propene, Ullmanns Encyclopedia of Industrial Chemistry, vol. A22, VCH, Weinheim, 1993, pp. 211–222.
[2] E.A. Mamedov, V. Cortés Corberan, Appl. Catal. A 127 (l) (1995).
[3] M.D. Argyle, K. Chen, A.T. Bell, E. Iglesia, J. Catal. 208 (2002) 139.
[4] B.M. Weckhuysen, D.E. Keller, Catal. Today 78 (2003) 25.
[5] A.A. Lemonidou, L. Nalbandian, I.A. Vasalos, Catal. Today 61 (2000) 333.
[6] G. Marta, F. Arena, S. Clouccia, F. Frusteri, A. Paramaliana, Catal. Today 63 (2000) 197.
[7] N. Steinfeldt, D. Müller, H. Berndt, Appl. Catal. A 272 (2004) 201.
[8] O. Schwarz, A. Dinse, B. Frank, R. Schomäcker, Catal. Commun., submitted for publication.
[9] E.V. Kondratenko, M. Cherian, M. Baerns, D. Su, R. Schlögl, X. Wang, I.E. Wachs, J. Catal. 234 (2005) 131.
[10] I.E. Wachs, Y. Chen, J.-M. Jehng, L.E. Briand, T. Tanaka, Catal. Today 78 (2003) 13.
[11] E.V. Kondratenko, M. Baerns, Appl. Catal. A 222 (2001) 133.
[12] R. Grabowski, Appl. Catal. A 270 (2004) 37.
[13] A. Bottino, G. Capannelli, A. Comite, S. Storace, R. Di Felice, Chem. Eng. J. 94 (2003) 11.
[14] R. Burch, E.M. Crabb, Appl. Catal. A 100 (1993) 111.
[15] P. Mars, D.W. van Krevelen, Spec. Suppl. Chem. Eng. Sci. 3 (1954) 41.
[16] K. Chen, A. Khodakov, J. Yang, A.T. Bell, E. Iglesia, J. Catal. 186 (1999) 325.
[17] A. Pantazidis, S.A. Bucholz, H.W. Zanthoff, Y. Schuurman, C. Mirodatos, Catal. Today 40 (1998) 207.
[18] K. Chen, A. Khodakov, J. Yang, A.T. Bell, E. Iglesia, J. Catal. 186 (1999) 325.
[19] E.V. Kondratenko, M. Cherian, M. Baerns, Catal. Today 99 (2005) 59.
[20] N. Ballarinia, F. Cavani, M. Ferraria, R. Catanic, U. Cornaro, J. Catal. 213 (2003) 95.
[21] S.L.T. Andersson, Appl. Catal. A 112 (1994) 209.
[22] K. Routray, G. Deo, AIChE J. 51 (2005) 1733.
[23] D. Creaser, B. Andersson, Appl. Catal. A 141 (1996) 131.
[24] J. Le Bars, A. Auroux, M. Forissier, J.C. Vedrine, J. Catal. 162 (1996) 250.
[25] I.E. Wachs, Catal. Today 27 (1996) 437.
[26] G. Deo, I.E. Wachs, J. Catal. 146 (1994) 323.
[27] A. Khodakov, B. Olthof, A.T. Bell, E. Iglesia, J. Catal. 181 (1999) 205.
[28] VDI-Gesellschaft Verfahrenstechnik und Chemieingenieurwesen (GVC), VDI-Wärmeatlas (VDI Heat Atlas), 3rd ed., Karlsruhe und Düsseldorf, 1977 (in German).
[29] H. Purnama, T. Ressler, R.E. Jentoft, H. Soerijanto, R. Schlögl, R. Schomäcker, Appl. Catal. A 259 (2004) 83.